

BaCuS₂: a superconductor with moderate electron-electron correlation

Yuhao Gu,¹ Xianxin Wu,¹ Kun Jiang,¹ and Jiangping Hu^{1,2,*}

¹Beijing National Laboratory for Condensed Matter Physics,
and Institute of Physics, Chinese Academy of Sciences, Beijing 100190, China

²CAS Center of Excellence in Topological Quantum Computation and Kavli Institute of Theoretical Sciences,
University of Chinese Academy of Sciences, Beijing 100190, China

We show that the layered-structure BaCuS₂ is a moderately correlated electron system in which the electronic structure of the CuS layer bears a resemblance to those in both cuprates and iron-based superconductors. Theoretical calculations reveal that the in-plane d - p σ^* -bonding bands are isolated near the Fermi level. As the energy separation between the d and p orbitals are much smaller than those in cuprates and iron-based superconductors, BaCuS₂ is expected to be moderately correlated. We suggest that this material is an ideal system to study the competitive/collaborative nature between two distinct superconducting pairing mechanisms, namely the conventional BCS electron-phonon interaction and the electron-electron correlation, which may be helpful to establish the elusive mechanism of unconventional high-temperature superconductivity.

I. INTRODUCTION

From conventional BCS superconductors to unconventional high T_c superconductors, cuprates[1], it has been widely suggested that the superconducting mechanism changes from phonon-mediated attraction to electron-electron correlation driving pairing. However, the existence of such a difference is still under intensive debate. For example, in the search of conventional BCS superconductors with relatively high transition temperature, a possible guiding principle is to find systems with metallized σ -bonding electrons from light atoms so that the electron-phonon interaction can be maximized[2–4]. Such a textbook example is MgB₂[2, 5, 6], in which the in-plane σ bands are formed by the p_x and p_y orbitals of B atoms. The Mg²⁺ ions further lower the B π (p_z) bands, which causes a charge transfer from σ to π bands and drives the self-doping of the σ band. The 2D nature of σ bonds then leads to an extremely large deformation potential for the in-plane E_{2g} phonon mode, which greatly enhances the electron-phonon coupling [2, 6]. This principle was also argued to be valid even for cuprates, in which the d - p σ -bonding band is responsible for superconductivity [4, 7]. The argument has left a room to discuss the likelihood of the electron-phonon mechanism in cuprates[8].

However, the d - p bonding displays fundamental differences from the p - p bonding because of the multiplicity and strong localization of the d -orbitals. Such a simple extension is highly questionable. For example, the absence of clear isotope effect [9], unconventional electronic properties in normal states and strongly antiferromagnetic fluctuations in cuprates suggest the electron-electron correlation can be responsible for high T_c superconductivity[10, 11]. Furthermore, the discovery of high T_c iron-based superconductors(SCs) finishes another large part of the superconducting jigsaw puzzle. Much evidence has suggested that the superconductivity of iron-based superconductors originates from the Fe-As/Te plane with strong electron-electron correlation and is very similar to cuprates[12–14]. On the other hand,

electron-phonon coupling also plays a non-negligible role in iron-based superconductors[15–17].

Recently, focusing on the d -orbitals, emphasizing electron-electron interaction, we have suggested a new guiding principle for the search of unconventional high T_c superconductors: those d -orbitals with d - p σ -bondings must be isolated near Fermi energy. Under this principle, local cation complexes, the connection between the complexes, the electron filling factor at transition metal atoms and lattice symmetries must collaborate to fulfill the criteria[18–22]. This simple principle can explain why cuprates and iron-based superconductors are so special as high T_c superconductors.

It is noticeable that the above mentioned two principles are linked. While they emphasize different interactions, both of them are featured by σ -bonding. Thus, why are the two types of σ -bonding fundamentally different? In order to answer these two questions, we want to find a system with a moderate electron-electron correlation from the d - p σ -bonding so that an explicit comparison between the electron-electron correlation and electron-phonon interaction can be examined.

In this paper, we propose that a new material BaCuS₂ can fulfill the above task. BaCuS₂ is a moderately correlated electron system in which the d - p σ^* -bonding bands solely control the electronic physics near Fermi energy. Similar to cuprates, iron pnictides and MgB₂, BaCuS₂ also has a layered structure, where the electronic structure is dominated by the CuS₂ square layer. We demonstrate that the electron-electron correlation may drive superconductivity in BaCuS₂ with a d_{xy} -wave pairing symmetry, very similar to the superconductivity in cuprates. While, if the superconductivity is caused by electron-phonon couplings, a conventional BCS s -wave state is expected, similar to La₃N₃Ni₂B₂. According to first-principles calculations, we find that the BaCuS₂ phase is thermodynamically stable and has lower formation energy under pressure compared with other known phases, suggesting that it can be synthesized in future experiments under external pressure.

* jphu@iphy.ac.cn

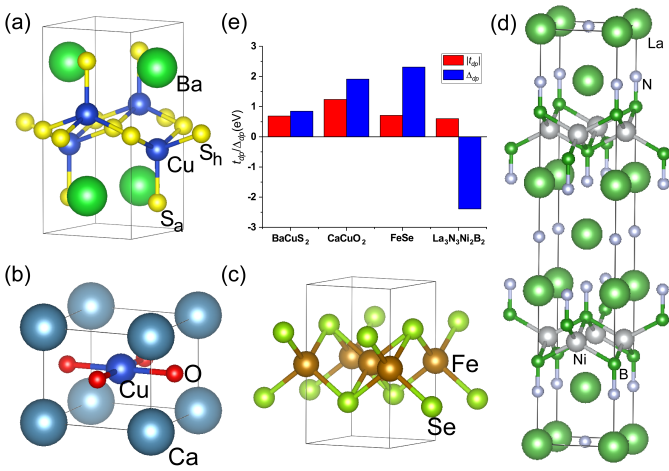


FIG. 1. (a) Crystal structure of BaCuS_2 . Here S_a represents the apical S atoms while S_h represents the horizontal S atoms. (b-d) Crystal structures of other layered superconductors (b) CaCuO_2 , (c) FeSe and (d) $\text{La}_3\text{N}_3\text{Ni}_2\text{B}_2$. (e) The comparison of parameters in dp -models of BaCuS_2 , CaCuO_2 , FeSe and $\text{La}_3\text{N}_3\text{Ni}_2\text{B}_2$. Here $|t_{dp}|$ is the amplitude of the major hopping parameter in each compound ($|t_{Cu,d_{x^2-y^2}} - S_h, p_{x/y}|$ in BaCuS_2 , $|t_{Cu,d_{x^2-y^2}} - O, p_{x/y}|$ in CaCuO_2 , $|t_{Fe,d_{xz/yz}} - Se, p_{x/y}|$ in FeSe and $|t_{Ni,d_{xz/yz}} - B, p_{x/y}|$ in $\text{La}_3\text{N}_3\text{Ni}_2\text{B}_2$) and Δ_{dp} is the corresponding on-site energy difference.

II. BaCuS_2 ELECTRONIC STRUCTURE AND COMPARISON WITH OTHER SC MATERIALS

We start from the crystal structure and electronic structure. The layered ternary transition metal sulfide BaCuS_2 has a structure: the BaS layers alternate with Cu_2S_2 layers and the transitional metal atom is in square pyramidal coordination, as shown in FIG.1(a). The upward-pointing square pyramids connect the downward-pointing ones by sharing edges, forming the glide symmetric Cu_2S_2 plane. Similar to other layered SCs, the main electronic structure of BaCuS_2 stems from its Cu_2S_2 layer. To demonstrate it, we carried out density functional theory calculations for BaCuS_2 . The electronic structure and density of states (DOS) of BaCuS_2 are plotted in FIG.2. The bands around the Fermi level are formed by the d - p valence manifold. Partially-filled d - p σ^* -bonding bands cross the Fermi level, where Cu $d_{x^2-y^2}$ orbitals strongly hybridize with in-plane S $p_{x/y}$ orbitals and Cu d_{z^2} orbitals strongly couple with apical S p_z orbitals. Owing to the planar nature of Cu $d_{x^2-y^2}$ orbitals and S $p_{x/y}$ orbitals, these bands have a weak dispersion along the k_z direction. In contrast, the bands from Cu d_{z^2} orbitals and apical S p_z orbitals exhibit a large dispersion. We expect that the SC of BaCuS_2 is mainly contributed from the 2D cylindrical Fermi surface, which is similar to the other layered SCs.

It is interesting to compare the electronic structure of BaCuS_2 with those of high- T_c superconductors (CaCuO_2 [23]; FeSe [24]) and known BCS superconductor ($\text{La}_3\text{N}_3\text{Ni}_2\text{B}_2$ [25]). These three materials are layered transition metal compounds, are shown in FIG.1(b-d). Their

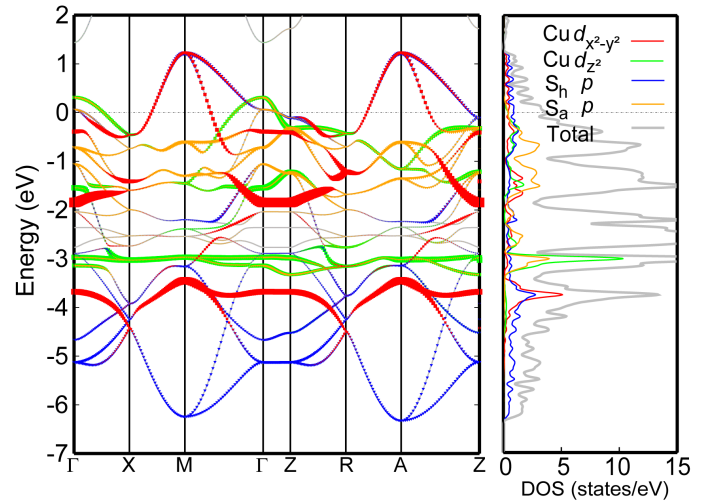


FIG. 2. The band structure and density of states for BaCuS_2 from density functional theory (DFT) calculation. The sizes of dots represent the weights of the projection. Here S_a represents the apical S atoms while S_h represents the horizontal S atoms.

electronic structures are mainly attributed to the square layers. In CaCuO_2 and FeSe , the electron correlation plays an important role in the unconventional superconductivity[19]. From an electronic-structure perspective, this is consistent with the fact that the d -orbitals dominate around the Fermi surfaces in these materials, giving rise to strong correlations. However, in $\text{La}_3\text{N}_3\text{Ni}_2\text{B}_2$, the extended s - p bands of anions dominate Fermi surfaces and are featured by strong electron-phonon couplings via B's high frequency A_{1g} phonons, while Ni's d -orbitals play a less pronounced role[26, 27]. As shown in FIG.2, in the d - p σ^* -bonding bands of BaCuS_2 near Fermi energy, the weight of p -orbitals of the in-plane S atoms is much larger than those in cuprates and iron-based superconductors. In contrast to $\text{La}_3\text{N}_3\text{Ni}_2\text{B}_2$, the weight of $d_{x^2-y^2}$ orbitals of Cu atoms is still sizable.

To quantitatively confirm this point, we construct tight-binding models including the d -orbitals of transition-metal atoms and the p -orbitals of coordinated anions to analyze their electronic structures by calculating the maximally localized Wannier functions (MLWFs)[28]. Our Wannierization results successfully reproduce the band structures from DFT calculations, as shown in appendix (FIG.S3). Then, we extract hopping parameters and on-site energies from our Wannierization results and display the representative parameters in appendix (TABLE.S1). In cuprate CaCuO_2 and iron-based superconductor FeSe , the electronic physics is dominated by d -orbitals near the Fermi level, whose on-site energies are much higher (about 2 eV) than those of coupled p -orbitals. Nevertheless, in BCS-type superconductor $\text{La}_3\text{N}_3\text{Ni}_2\text{B}_2$, where the NiB layer is isostructural to the FeSe layer, the electronic physics is quite distinct: the on-site energy of B- $p_{x/y}$ orbital is even higher than that of Ni- $d_{xz/yz}$ orbital. This is consistent with previous studies[26, 27]: multiple components cross the Fermi level, showing that $\text{La}_3\text{N}_3\text{Ni}_2\text{B}_2$ is a good metal. The scenario of BaCuS_2 is different from above examples: the on-site en-

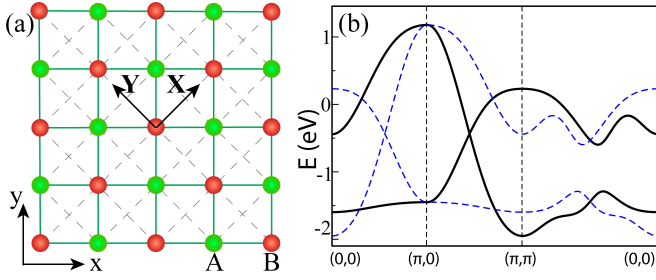


FIG. 3. (color online) (a) Lattice structure of Cu layer in the tight-binding model. In each unit cell, there are two Cu atoms sitting above and below the xy plane. We label these two sublattices by A and B, respectively. The conventional crystal structure direction is defined for Cu_A to Cu_A direction, labeled as $X - Y$. To simplify our model using glide symmetry, we rotate the global axis to Cu_A to Cu_B direction, labeled as $x-y$. (b) The two-Cu tight-binding model for BaCuS_2 in Eq.(1) (black lines). The blue dash lines are the folded energy bands with a folding vector $\mathbf{Q}=(\pi, \pi)$.

ergies of d -orbitals are still higher than the p -orbitals, but the energy difference is only about 1 eV, much less than those in high- T_c superconductors. It suggests that the antiferromagnetic (AFM) order may not be stabilized in BaCuS_2 due to the weak superexchange coupling [29]. Moreover, the difference in hopping parameters between partially-filled d -orbitals and coupled p -orbital is not so significant, as shown in FIG.1.(b).

The above analysis in BaCuS_2 is consistent with the absence of any magnetically ordered states in our calculation. Therefore, BaCuS_2 tends to be a material with a moderate electron-electron correlation.

As mentioned previously, the guiding principle for searching high transition temperature BCS superconductors are light atoms and metallized σ -bonding electrons[2, 3]. In principle, in BaCuS_2 , the d - p σ^* -bonding bands cross the Fermi level, where those metallic σ -bonding electrons can support the BCS-type superconductivity. Thus, we calculate the electron-phonon coupling (EPC) properties of BaCuS_2 [28]. The EPC strength λ is about 0.59 in BaCuS_2 , which is lower than that in $\text{La}_3\text{N}_3\text{Ni}_2\text{B}_2$ ($\lambda \sim 0.86$, $T_c \sim 13\text{K}$ [30]) but slightly higher than that in LaNiBN ($\lambda \sim 0.52$, $T_c \sim 4.1\text{K}$ [31]). However, due to the heavy mass of Cu and S atoms, we find that the electron-phonon coupling in BaCuS_2 can only induce superconductivity of T_c less than 4 K.[28].

TABLE I. The optimized structural parameters for BaCuS_2 (space group $P4/nmm$). Here S_a represents the apical S atoms while S_h represents the horizontal S atoms.

System	a(Å)	c(Å)	Cu- S_h (Å)	Cu- S_a (Å)	Cu- S_h -Cu($^\circ$)
BaCuS_2	4.49	9.14	2.41	2.32	97.6

III. THE EFFECTIVE TWO BAND MODEL AND RPA RESULTS

To study the correlation effect, we first construct an effective minimal model by Wannierization based on the $d_{x^2-y^2}$ -like and d_{z^2} -like MLWFs on Cu sites in BaCuS_2 [28, 32, 33]. The d - p σ^* -bonding bands are obviously more delocalized in BaCuS_2 than that in CaCuO_2 (More details can be found in appendix FIG.S4.(c-e)). As a consequence, the correlation strength in BaCuS_2 should be weaker. Then by fitting the Wannierization results[28], we arrive at an effective tight-binding (TB) model in the basis of $d_{x^2-y^2}$ orbital and d_{z^2} orbital.

There are two Cu atoms in each unit cell, as shown in FIG.3(a), which indicates that the minimal model for BaCuS_2 contains four bands. Similar to FeSe, the space group of BaCuS_2 is $P4/nmm$. There is a glide symmetry which consists of a translation Cu_A to Cu_B and a mirror reflection perpendicular to the S plane. Then, using glide symmetry, one can unfold the band structure into the Brillouin zone of one-Cu unit cell and write down a two-band model for BaCuS_2 . Note that, the conventional crystal structure direction of BaCuS_2 is defined for the Cu_A to Cu_A direction, labeled as $X - Y$. Similar to iron based superconductors, we define a new coordinate system with the x and y axes aligned to the Cu_A to Cu_B direction, labeled as $x-y$ [34, 35].

The two-band model in one-Cu unit cell in the basis $\psi_k = (d_{z^2}(k), d_{X^2-Y^2}(k))$ (the spin index is omitted here) can be written as

$$H = \sum_k \psi_k^\dagger \hat{H}_k \psi_k \quad (1)$$

where the 2 by 2 matrix H_k and more details are provided in appendix. The band structure in the original unit cell can be obtained by the folding the band structures of the Hamiltonian H_k , as plotted in FIG.3(b), where the blue dash lines are folded bands with a folding vector $\mathbf{Q}=(\pi, \pi)$. The corresponding FSs are displayed in Fig.4(d) and the large oval FSs around $(\pi, 0)$ or $(0, \pi)$ are mainly attributed to $d_{X^2-Y^2}$ orbital while the smaller circular FS around the M point is mainly attributed to d_{z^2} orbitals.

Using the above two-band model, we can apply the standard approach to investigate the intrinsic spin fluctuations by carrying out RPA calculation[36–40]. We adopt the general multi-orbital Coulomb interactions, including on-site Hubbard intra- and inter-orbital repulsion U/U' , Hund's coupling J and pairing interactions J' ,

$$\begin{aligned}
 H_{int} = & U \sum_{i\alpha} n_{i\alpha\uparrow} n_{i\alpha\downarrow} + U' \sum_{i,\alpha<\beta} n_{i\alpha} n_{i\beta} \\
 & + J \sum_{i,\alpha<\beta,\sigma\sigma'} c_{i\alpha\sigma}^\dagger c_{i\beta\sigma'}^\dagger c_{i\alpha\sigma'} c_{i\beta\sigma} \\
 & + J' \sum_{i,\alpha\neq\beta} c_{i\alpha\uparrow}^\dagger c_{i\alpha\downarrow}^\dagger c_{i\beta\downarrow} c_{i\beta\uparrow}, \quad (2)
 \end{aligned}$$

where $n_{i\alpha} = n_{i\alpha\uparrow} + n_{i\alpha\downarrow}$. The distribution of the largest eigenvalues of bare susceptibility matrices is displayed in Fig.4(a). There is a prominent peak at q_1 , close to $(\frac{\pi}{2}, 0)$.

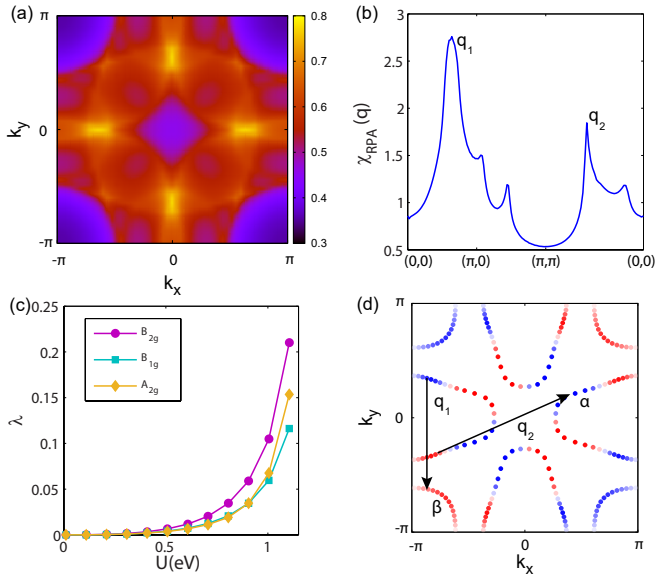


FIG. 4. (color online) (a) Distribution of the largest eigenvalues for bare susceptibility matrices $\chi_0(\mathbf{k})$ at $n = 2.0$. (b) Largest eigenvalues of RPA susceptibility with $U = 0.9$ eV and $J/U = 0.2$. (c) Pairing strength eigenvalues for the leading states as a function of interaction U with $J/U = 0.2$. (d) Gap function of the dominant B_{2g} state (d_{xy} -wave pairing).

In addition, the bare susceptibility shows a broad peak at q_2 . The former is attributed to the inter-pocket nesting between α and β and the latter is contributed by intra pocket nesting in α Fermi surface. From the RPA spin susceptibility along high-symmetry lines shown in Fig.4(b), we find that these peaks get significantly enhanced when interactions are included. All peaks in the susceptibility are far away from the Γ point, indicating intrinsic antiferromagnetic fluctuations in the system. To investigate the pairing symmetry, we calculate the pairing strengths as a function of Coulomb interaction U with $J/U = 0.2$. The dominant pairing has a B_{2g} symmetry, whose gap function is shown in Fig.4(d). Each pocket has a d_{xy} -wave gap but the intrapocket nesting in α pockets induces additional sign changes in the corresponding gap functions. Moreover, there is a sign change between the gap functions on α and β pockets, which is determined by inter pocket nesting. The gap functions on these Fermi surfaces can be qualitatively described by a form factor $\text{sink}_x \text{sink}_y (\cos k_x + \cos k_y)$, which is classified as the d_{xy} (B_{2g}) pairing symmetry. In this superconducting state, there are gapless nodes on high symmetry lines as well as nodes on the original BZ boundary.

The d_{xy} pairing symmetry is quite robust here. In fact, if we consider the system in a strong electron-electron correlation region in which a short AFM interaction can be produced through the superexchange mechanism. We can easily argue that the pairing symmetry in this limit is still d_{xy} based on the Hu-Ding principle[41] which states the pairing symmetry is selected by the momentum space form factor of AFM exchange couplings that produce the largest weight on Fermi surfaces. In this case, we would expect the gap function is proportional to $\text{sink}_x \text{sink}_y$, in which the nodal points at the

TABLE II. The optimized volumes of BaCuS_2 , $\text{Ba}_3\text{Cu}_2\text{S}_5$ and their decomposition phases under different pressures. All the data are normalized according to the formula. The unit of volume is \AA^3 here.

	0 GPa	5 GPa	10 GPa	15 GPa	20 GPa
BaCuS_2	92.07	85.29	80.50	76.73	73.78
$\text{BaS}+\text{CuS}$	101.41	93.42	87.99	83.89	80.55
$\text{Ba}_3\text{Cu}_2\text{S}_5$	253.46	234.47	220.87	210.59	202.20
$3\text{BaS}+2\text{CuS}$	270.09	247.89	232.96	221.74	212.65

BZ boundary in the above RPA calculations will not appear.

IV. DISCUSSION AND SUMMARY

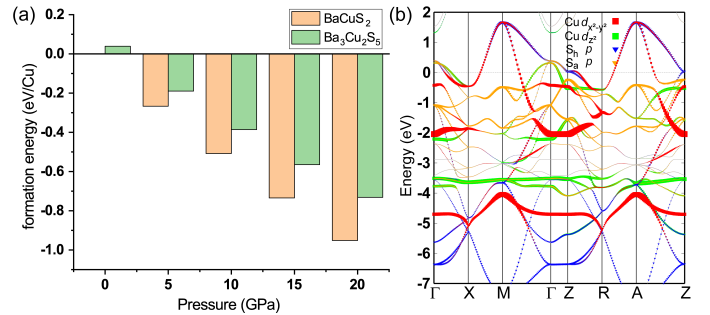


FIG. 5. (a) Formation energies of BaCuS_2 and $\text{Ba}_3\text{Cu}_2\text{S}_5$ under different pressures. (b) The band structure of BaCuS_2 with an external pressure $P = 20$ GPa from DFT calculation. The sizes of dots represent the weights of the projection.

In summary, we propose a new superconducting material BaCuS_2 . By comparing the electronic structures with CaCuO_2 , FeSe and $\text{La}_3\text{N}_3\text{Ni}_2\text{B}_2$, we find that BaCuS_2 should be a moderately correlated electron system with strong $p-d$ hybridization. The calculations based conventional BCS electron-phonon coupling suggests that it is a standard s -wave superconductor with $T_c < 4$ K, while the electron-electron correlation results in an unconventional B_{2g} -wave superconductor and possibly much higher T_c .

The structure of the material is in a highly stable phase according to our theoretical calculations. In particular, we find that the structure has much lower formation energy than other known structures under external pressure. We calculate the formation energy of BaCuS_2 and its sister compound $\text{Ba}_3\text{Cu}_2\text{S}_5$ [42] under different pressures, as shown in FIG.5.(a). The volume of $\text{BaCuS}_2/\text{Ba}_3\text{Cu}_2\text{S}_5$ is remarkably less than that of $\text{BaS}+\text{CuS}/3\text{BaS}+2\text{CuS}$, as shown in TABLE.II. The main electronic physics does not vary much under pressure as shown in FIG.5.(b), in which the band structure of BaCuS_2 under 20 GPa is plotted. Therefore, it is promising that BaCuS_2 can be synthesized in future experiments and studying its superconductivity can help us reveal the relationship between conventional and unconventional superconducting mechanisms.

Acknowledgement: We thank the useful discussions with

Jianfeng Zhang and Yuechao Wang. This work is supported by the Ministry of Science and Technology of China 973 pro-

gram (No. 2017YFA0303100), National Science Foundation of China (Grant No. NSFC11888101), and the Strategic Priority Research Program of CAS (Grant No.XDB28000000).

-
- [1] P. A. Lee, N. Nagaosa, and X.-G. Wen, *Rev. Mod. Phys.* **78**, 17 (2006).
- [2] J. M. An and W. E. Pickett, *Phys. Rev. Lett.* **86**, 4366 (2001).
- [3] M. Gao, Z.-Y. Lu, and T. Xiang, *Physical Review B* **91**, 045132 (2015).
- [4] M. Gao, Z.-Y. Lu, and T. Xiang, *PHYSICS (in Chinese)* **44**, 421 (2015).
- [5] J. Kortus, I. I. Mazin, K. D. Belashchenko, V. P. Antropov, and L. L. Boyer, *Phys. Rev. Lett.* **86**, 4656 (2001).
- [6] X. X. Xi, *Rep. Prog. Phys.* **71**, 116501 (2008).
- [7] F. Zhang and T. Rice, *Physical Review B* **37**, 3759 (1988).
- [8] Y. Zhong, Y. Wang, S. Han, Y.-F. Lv, W.-L. Wang, D. Zhang, H. Ding, Y.-M. Zhang, L. Wang, K. He, *et al.*, *Science Bulletin* **61**, 1239 (2016).
- [9] J. Franck, *Physical Properties of High-Temperature Superconductivity (Vol 4)* (Singapore: World Scientific, 1994).
- [10] A. Millis, H. Monien, and D. Pines, *Physical Review B* **42**, 167 (1990).
- [11] D. J. Scalapino, *Physics Reports* **250**, 329 (1995).
- [12] P. Dai, J. Hu, and E. Dagotto, *Nature Physics* **8**, 709 (2012).
- [13] K. Seo, B. A. Bernevig, and J. Hu, *Physical review letters* **101**, 206404 (2008).
- [14] Q. Si and E. Abrahams, *Physical Review Letters* **101**, 076401 (2008).
- [15] R. Liu, T. Wu, G. Wu, H. Chen, X. Wang, Y. Xie, J. Ying, Y. Yan, Q. Li, B. Shi, *et al.*, *Nature* **459**, 64 (2009).
- [16] S. Rebec, T. Jia, C. Zhang, M. Hashimoto, D.-H. Lu, R. Moore, and Z.-X. Shen, *Physical review letters* **118**, 067002 (2017).
- [17] W. Qiong, Z. Huaxue, W. Yanling, H. Lili, N. Shunli, T. Yichao, S. Fei, Z. Fang, D. Xiaoli, Z. Zhongxian, *et al.*, *Chinese Physics Letters* **37**, 97802 (2020).
- [18] J. Hu, C. Le, and X. Wu, *Physical Review X* **5**, 041012 (2015).
- [19] J. Hu, *Sci. Bull.* **61**, 561 (2016).
- [20] C. Le, J. Zeng, Y. Gu, G.-H. Cao, and J. Hu, *Science Bulletin* **63**, 957 (2018).
- [21] J. Hu, Y. Gu, and C. Le, *Science Bulletin* **63**, 1338 (2018).
- [22] Y. Gu, Q. Zhang, C. Le, Y. Li, T. Xiang, and J. Hu, *Physical Review B* **100**, 165405 (2019).
- [23] M. Azuma, Z. Hiroi, M. Takano, Y. Bando, and Y. Takeda, *Nature* **356**, 775 (1992).
- [24] F.-C. Hsu, J.-Y. Luo, K.-W. Yeh, T.-K. Chen, T.-W. Huang, P. M. Wu, Y.-C. Lee, Y.-L. Huang, Y.-Y. Chu, D.-C. Yan, *et al.*, *Proceedings of the National Academy of Sciences* **105**, 14262 (2008).
- [25] R. Cava, H. Zandbergen, B. Batlogg, H. Eisaki, H. Takagi, J. Krajewski, W. Peck, E. Gyorgy, and S. Uchida, *Nature* **372**, 245 (1994).
- [26] L. Mattheiss, *Solid state communications* **94**, 741 (1995).
- [27] D. J. Singh and W. E. Pickett, *Phys. Rev. B* **51**, 8668 (1995).
- [28] Please find more details in our appendix.
- [29] In our DFT+ U calculations, antiferromagnetism always quenches ($U = 0 \sim 10eV$) in $BaCuS_2$.
- [30] C. K. Poole, H. A. Farach, and R. J. Creswick, *Handbook of superconductivity* (Elsevier, 1999).
- [31] M.-C. Jung, C.-J. Kang, B. Min, and K.-W. Lee, *Physical Review B* **87**, 144509 (2013).
- [32] A. A. Mostofi, J. R. Yates, Y.-S. Lee, I. Souza, D. Vanderbilt, and N. Marzari, *Comput. Phys. Commun.* **178**, 685 (2008).
- [33] N. Marzari, A. A. Mostofi, J. R. Yates, I. Souza, and D. Vanderbilt, *Rev. Mod. Phys.* , 1419 (2012).
- [34] J. Hu and N. Hao, *Physical Review X* **2**, 021009 (2012).
- [35] N. Hao and J. Hu, *Physical Review X* **4**, 031053 (2014).
- [36] S. Graser, T. Maier, P. Hirschfeld, and D. Scalapino, *New Journal of Physics* **11**, 025016 (2009).
- [37] A. F. Kemper, T. A. Maier, S. Graser, H.-P. Cheng, P. Hirschfeld, and D. Scalapino, *New Journal of Physics* **12**, 073030 (2010).
- [38] X. Wu, J. Yuan, Y. Liang, H. Fan, and J. Hu, *EPL (Europhysics Letters)* **108**, 27006 (2014).
- [39] X. Wu, F. Yang, C. Le, H. Fan, and J. Hu, *Physical Review B* **92**, 104511 (2015).
- [40] D. Di Sante, X. Wu, M. Fink, W. Hanke, and R. Thomale, *Physical Review B* **99**, 201106 (2019).
- [41] J. Hu and H. Ding, *Sci. Rep.* **2**, 381 (2012).
- [42] $Ba_3Cu_2S_5$ shares similar electronic physics with $BaCuS_2$, and Cu is also in square pyramidal coordination. Please find more details in our appendix.
- [43] G. Kresse and J. Furthmüller, *Phys. rev. B* **54**, 11169 (1996).
- [44] G. Kresse and D. Joubert, *Phys. Rev. B* **59**, 1758 (1999).
- [45] J. P. Perdew, K. Burke, and M. Ernzerhof, *Phys. Rev. Lett.* **77**, 3865 (1996).
- [46] S. Poncé, E. R. Margine, C. Verdi, and F. Giustino, *Computer Physics Communications* **209**, 116 (2016).
- [47] P. Giannozzi, S. Baroni, N. Bonini, M. Calandra, R. Car, C. Cavazzoni, D. Ceresoli, G. L. Chiarotti, M. Cococcioni, I. Dabo, *et al.*, *Journal of physics: Condensed matter* **21**, 395502 (2009).
- [48] N. Troullier and J. L. Martins, *Physical review B* **43**, 1993 (1991).
- [49] D. Hamann, *Physical Review B* **88**, 085117 (2013).
- [50] M. Schlipf and F. Gygi, *Computer Physics Communications* **196**, 36 (2015).
- [51] P. B. Allen, *Physical Review B* **6**, 2577 (1972).
- [52] P. B. Allen and R. Dynes, *Physical Review B* **12**, 905 (1975).
- [53] Y. Gu, S. Zhu, X. Wang, J. Hu, and H. Chen, *Communications Physics* **3**, 1 (2020).
- [54] Y.-C. Wang and H. Jiang, *The Journal of chemical physics* **150**, 154116 (2019).
- [55] Y. Klein, M. Casula, D. Santos-Cottin, A. Audouard, D. Vignolles, G. Feve, V. Freulon, B. Placais, M. Verseils, H. Yang, *et al.*, *Physical Review B* **97**, 075140 (2018).
- [56] D. Santos-Cottin, A. Gauzzi, M. Verseils, B. Baptiste, G. Feve, V. Freulon, B. Placais, M. Casula, and Y. Klein, *Physical Review B* **93**, 125120 (2016).
- [57] N. Berk and J. Schrieffer, *Physical Review Letters* **17**, 433 (1966).
- [58] D. Scalapino, E. Loh Jr, and J. Hirsch, *Physical Review B* **34**, 8190 (1986).
- [59] T. Takimoto, T. Hotta, and K. Ueda, *Physical Review B* **69**, 104504 (2004).
- [60] K. Kubo, *Physical Review B* **75**, 224509 (2007).

Appendix A: Computational methods

Our electronic structure calculations employ the Vienna ab initio simulation package (VASP) code[43] with the projector augmented wave (PAW) method[44]. The Perdew-Burke-Ernzerhof (PBE)[45] exchange-correlation functional is used in our calculations. The kinetic energy cutoff is set to be 600 eV for the expanding the wave functions into a plane-wave basis in VASP calculations. For body centered tetragonal $\text{La}_3\text{N}_3\text{Ni}_2\text{B}_2$ and $\text{Ba}_3\text{Cu}_2\text{S}_5$, we employ their primitive cells to perform calculations. In the calculations of the formation energy, the energy convergence criterion is 10^{-6} eV and the force convergence criterion is 0.01 eV/Å. The Γ -centered \mathbf{k} -meshes are $16 \times 16 \times 8$, $6 \times 6 \times 6$, $16 \times 16 \times 16$, $18 \times 18 \times 4$, $18 \times 18 \times 22$, $20 \times 20 \times 12$ and $8 \times 8 \times 8$ for BaCuS_2 , $\text{Ba}_3\text{Cu}_2\text{S}_5$, BaS , CuS , CaCuO_2 , FeSe and $\text{La}_3\text{N}_3\text{Ni}_2\text{B}_2$, respectively.

We employ Wannier90[32, 33] to calculate maximally localized Wannier functions in BaCuS_2 , CaCuO_2 , FeSe and $\text{La}_3\text{N}_3\text{Ni}_2\text{B}_2$. In the calculations of the d - p models, the initial projectors are transition metal atoms' d -orbitals and anions' p -orbitals in BaCuS_2 , CaCuO_2 and FeSe . For $\text{La}_3\text{N}_3\text{Ni}_2\text{B}_2$, the Ni(d)-B(p) valence manifold strongly entangles with other bands, so La's d -orbitals and B's s -orbitals are added in its initial projectors to reproduce DFT-calculated band structures. In the calculation of the d - p σ^* MLWFs, the initial projectors are Cu's $d_{x^2-y^2} + d_{z^2}$ orbitals in BaCuO_2 and Cu's $d_{x^2-y^2}$ orbital in CaCuO_2 , respectively.

We employ EPW package[46] to calculate the electron-phonon coupling properties of BaCuS_2 . The MLWFs are calculated by Wannier90[32, 33] interfacing with Quantum ESPRESSO[47]. We take the $16 \times 16 \times 8$ \mathbf{k} -mesh and $4 \times 4 \times 2$ \mathbf{q} -mesh as coarse grids and then interpolate to the $64 \times 64 \times 32$ \mathbf{k} -mesh and $8 \times 8 \times 4$ \mathbf{q} -mesh. The kinetic energy cutoff is set to 80 Ry. The Gaussian smearing method with the width of 0.005 Ry is used for the Fermi surface broadening. The energy convergence criterion is 10^{-12} eV. In the highly accurate structural optimization, the lattice constants and atomic coordinates are relaxed and the force convergence criterion is 0.000001 Ry/Bohr. The exchange-correlation functional is also PBE and the norm-conserving SG15 pseudopotentials are used[48–50].

Appendix B: electron-phonon properties of BaCuS_2

The phonon density of states $F(\omega)$ and the corresponding Eliashberg spectral function $\alpha^2F(\omega)$ are plotted in FIG.S1.(a). By intergating $\alpha^2F(\omega)$, we get a moderate EPC strength $\lambda = 0.59$. We estimate the superconducting transition temperature T_c with the McMillan-Allen-Dynes formula[51, 52],

$$T_c = \frac{\omega_{\log}}{1.2} \exp \left[\frac{-1.04(1 + \lambda)}{\lambda(1 - 0.62\mu^*) - \mu^*} \right], \quad (\text{B1})$$

where μ^* is the effective screened Coulomb repulsion constant and the logarithmic average of the Eliashberg spectral

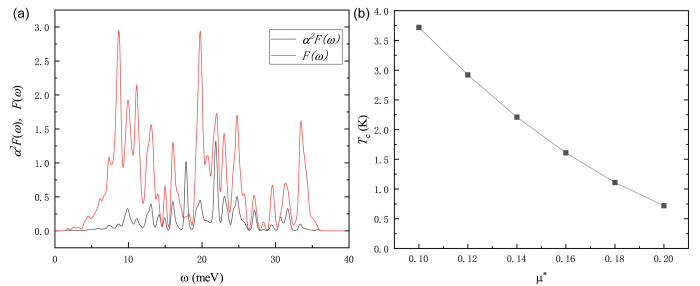


FIG. S1. (a) Eliashberg spectral function $\alpha^2F(\omega)$ (red line) and Phonon density of states $F(\omega)$ (black line) for BaCuS_2 . (b) Evaluated T_c as a function of μ^* for BaCuS_2 .

function ω_{\log} is defined as

$$\omega_{\log} = \exp \left[\frac{2}{\lambda} \int \frac{d\omega}{\omega} \alpha^2F(\omega) \ln(\omega) \right]. \quad (\text{B2})$$

As μ^* is an input parameter, we plot T_c as a function of μ^* in FIG.S1.(b). The phonon-mediated T_c for BaCuS_2 should be less than 4 K.

Appendix C: $\text{Ba}_3\text{Cu}_2\text{S}_5$: separation by three rock salt-type BaS layers

As shown in FIG.S2, the crystal structure of $\text{Ba}_3\text{Cu}_2\text{S}_5$ is similar to that of BaCuS_2 : The inverse α -PbO-type Cu_2S_2 layer is separated by 3 rock salt-type BaS layers in $\text{Ba}_3\text{Cu}_2\text{S}_5$ but separated by 2 BaS layers in BaCuS_2 ($\text{Ba}_2\text{Cu}_2\text{S}_4$). It also shares a similar electronic structure with BaCuS_2 , as shown in FIG.S2.(b). $\text{Ba}_3\text{Cu}_2\text{S}_5$ is not thermodynamically stable, but it is possible to synthesized $\text{Ba}_3\text{Cu}_2\text{S}_5$ under external pressure due to Cu's five-coordination, as shown in FIG.5.(a).

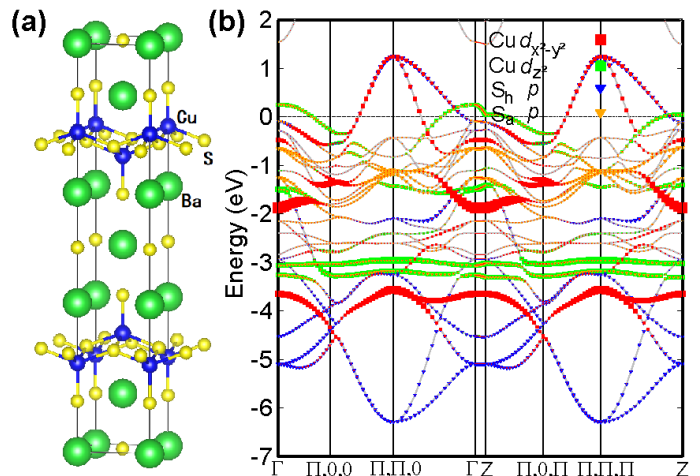


FIG. S2. (a) The crystal structure of $\text{Ba}_3\text{Cu}_2\text{S}_5$. (b) The band structure of BaCuS_2 with its primitive cell from DFT calculation. The sizes of dots represent the weights of the projection. Here S_a represents the apical S atoms while S_b represents the horizontal S atoms. The choice of the \mathbf{k} -path is same as the literature's[27].

Appendix D: Wannierization projected by d -orbitals and p -orbitals

Our Wannierization results successfully reproduce DFT-calculated band structures, as shown in FIG.S3. The relevant representative hopping parameters and on-site energies are listed in TABLE.S1. Here we use the conventional notations of the local crystal field coordinations.

TABLE S1. The hopping parameters and on-site energies for BaCuS₂, CaCuO₂, FeSe and La₃N₃Ni₂B₂. Here S_a represents the apical S atoms while S_h represents the horizontal S atoms.

BaCuS₂	
$\varepsilon_{Cu,d_{z^2}}$	-2.21
$\varepsilon_{Cu,d_{x^2-y^2}}$	-2.23
$\varepsilon_{Cu,d_{xz/yz}}$	-2.32
$\varepsilon_{Cu,d_{xy}}$	-2.48
ε_{S_h,p_z}	-2.58
$\varepsilon_{S_h,p_x/y}$	-3.08
ε_{S_a,p_z}	-2.17
$\varepsilon_{S_a,p_x/y}$	-1.40
$ t_{Cu,d_{x^2-y^2}-S_h,p_z} $	0.37
$ t_{Cu,d_{x^2-y^2}-S_h,p_x/y} $	0.69
$ t_{Cu,d_{z^2}-S_h,p_z} $	0.39
$ t_{Cu,d_{z^2}-S_h,p_x/y} $	0.11
$ t_{Cu,d_{z^2}-S_a,p_z} $	0.82
$ t_{S_a,p_x-S_a,p_x} $	0.09
CaCuO₂	
$\varepsilon_{Cu,d_{z^2}}$	-2.42
$\varepsilon_{Cu,d_{x^2-y^2}}$	-1.92
ε_{O,p_z}	-2.58
$\varepsilon_{O,p_x/y}$	-3.83
$ t_{Cu,d_{x^2-y^2}-O,p_x/y} $	1.24
FeSe	
$\varepsilon_{Fe,d_{x^2-y^2}}$	-0.88
$\varepsilon_{Fe,d_{xz/yz}}$	-0.78
ε_{Se,p_z}	-3.07
$\varepsilon_{Se,p_x/y}$	-3.09
$ t_{Fe,d_{x^2-y^2}-Se,p_x/y} $	0.25
$ t_{Fe,d_{x^2-y^2}-Se,p_z} $	0.72
$ t_{Fe,d_{xz/yz}-Se,p_x/y} $	1.00
$ t_{Fe,d_{x^2-y^2}-Se,p_z} $	0.16
La₃N₃Ni₂B₂	
$\varepsilon_{Ni,d_{z^2}}$	-2.11
$\varepsilon_{Ni,d_{x^2-y^2}}$	-2.26
$\varepsilon_{Ni,d_{xz/yz}}$	-2.11
$\varepsilon_{Ni,d_{xy}}$	-2.24
$\varepsilon_{B,s}$	0.23
ε_{B,p_z}	2.17
$\varepsilon_{B,p_x/y}$	0.28
$ t_{Ni,d_{x^2-y^2}-Ni,p_x/y} $	0.55
$ t_{Ni,d_{x^2-y^2}-Ni,p_z} $	0.78
$ t_{Ni,d_{xz/yz}-Ni,p_x/y} $	0.85
$ t_{Ni,d_{x^2-y^2}-Ni,p_z} $	0.27

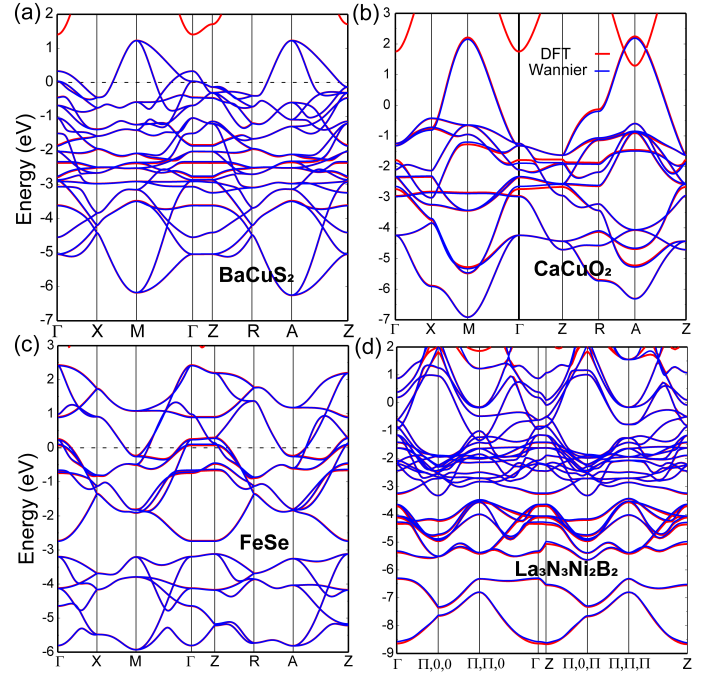


FIG. S3. The band structures of (a) BaCuS₂, (b) CaCuO₂, (c) FeSe and (d) La₃N₃Ni₂B₂. The red/blue lines represent DFT/Wannierization results, respectively. The choice of the k-path in (d) is same as the literature's[27].

Appendix E: Wannierization of the d - p σ^* -bonding bands and the effective tight-binding model

As mentioned above, the in-plane d - p σ^* -bonding bands are isolated around the Fermi surface. In order to construct the effective minimal model to describe the in-plane electronic physics in BaCuS_2 , we downfold the full $d-p$ model into an effective minimal model[53] by only Wannierizing the $d_{X^2-Y^2}$ -like and d_{z^2} -like MLWFs in BaCuS_2 with a smaller energy window. Our Wannierization results cap-

ture the main characters of BaCuS_2 's electronic structure, as shown in FIG.S4.(a). This is an analogy to the Zhang-Rice singlet in cuprates[7], so we also calculate the $d_{X^2-Y^2}$ -like MLWF in CaCuO_2 for comparison, as shown in FIG.S4.(b).

We construct the effective tight-binding (TB) model in the basis of $d_{X^2-Y^2}$ orbital and d_{z^2} orbital to describe the in-plane electronic physics. Since there are two Cu atoms in one unit cell, the TB model can be written as a 4×4 Hermitian matrix:

$$\begin{aligned}
 H_{11} &= H_{33} = \varepsilon_1 + 2t_{11}^x(\cos(k_x) + \cos(k_y)) + 2t_{11}^{xx}(\cos(2k_x) + \cos(2k_y)) + 4t_{11}^{xy}(\cos(k_x)\cos(k_y)), \\
 H_{12} &= H_{34} = 2t_{12}^x(\cos(k_x) - \cos(k_y)) + 2t_{12}^{xx}(\cos(2k_x) - \cos(2k_y)), \\
 H_{13} &= 4t_{13}^{xy}\cos(k_x/2)\cos(k_y/2) + 4t_{13}^{xy}(\cos(k_x/2) * \cos(3k_y/2) + \cos(3k_x/2)\cos(k_y/2)), \\
 H_{14} &= H_{23} = 4t_{14}^{xy}(\cos(3k_x/2)\cos(k_y/2) - \cos(k_x/2)\cos(3k_y/2)), \\
 H_{22} &= H_{44} = \varepsilon_2 + 2t_{22}^x(\cos(k_x) + \cos(k_y)) + 2t_{22}^{xx}(\cos(2k_x) + \cos(2k_y)) + 4t_{22}^{xy}(\cos(k_x)\cos(k_y)), \\
 H_{24} &= 4t_{24}^{xy}\cos(k_x/2)\cos(k_y/2) + 4t_{24}^{xy}(\cos(k_x/2) * \cos(3k_y/2) + \cos(3k_x/2)\cos(k_y/2)).
 \end{aligned}
 \tag{E1}$$

The hopping parameters are truncated to the fifth-nearest-neighbour site. We get hopping parameters and on-site energies by fitting to the Wannierization result in $k_z = 0$ plane, as shown in FIG.S6. The corresponding parameters and their notations are listed in TABLE.S2. The major hopping parameter is t_{11}^x , the intra-orbital hopping between two SNN $d_{X^2-Y^2}$ orbital, which is in the same energy scale with the dominating intra-orbital hopping between two NN $d_{x^2-y^2}$ orbital in cuprates ($t_{d_{x^2-y^2}}^{NN}$ is about -0.47 in CaCuO_2).

As mentioned in our main text, we can transfer the 4×4 TB model into a block-diagonalized matrix with using the glide symmetry:

$$H_{eff}(\mathbf{k}) = \begin{pmatrix} H_k & 0 \\ 0 & H_{k+Q} \end{pmatrix}, \tag{E2}$$

here H_k is the effective two-band model in our main text and $Q = (\pi, \pi)$. The explicit form of H_k is

$$H_k = \begin{pmatrix} H_{11} + H_{31} & H_{12} + H_{32} \\ H_{21} + H_{41} & H_{22} + H_{42} \end{pmatrix}, \tag{E3}$$

where $H_{\alpha\beta}$ are matrix elements in Eq.E1.

Visually, we plot these d - p σ^* Wannier functions in BaCuS_2 and CaCuO_2 , as shown in FIG.S4.(c-e). These Wannier functions are composed of Cu's d -orbitals and coordinated S/O's p -orbitals symmetrically. As the isovalues of isosurfaces in FIG.S4.(c-e) are same, the d - p σ^* -bonding bands are more delocalized in BaCuS_2 than that in CaCuO_2 . As a result, the correlation strength in BaCuS_2 should be weaker.

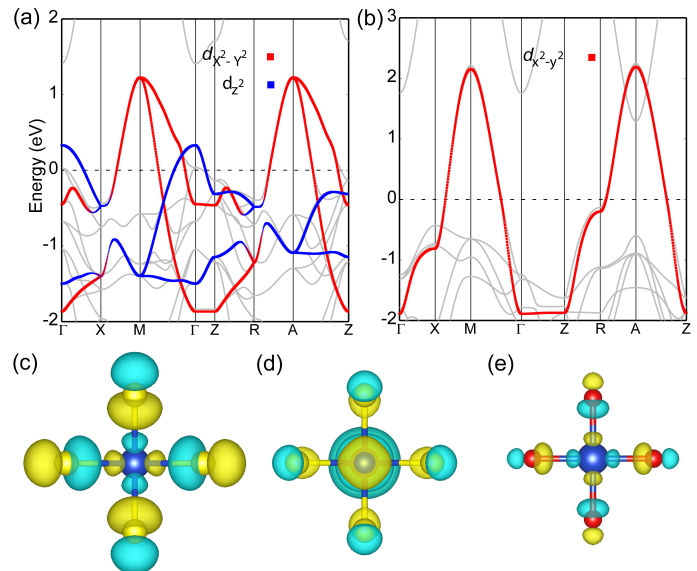


FIG. S4. (a-b) The band structures of (a) BaCuS_2 and (b) CaCuO_2 calculated by DFT (gray lines) and Wannierization (red/blue dots). The sizes of dots represent the weights of the projection of the d - p σ^* Wannier functions. (c-d) The isosurface of (c) the $d_{X^2-Y^2}$ -like MLWF and (d) the d_{z^2} -like MLWF in BaCuS_2 . (e) The isosurface of the $d_{x^2-y^2}$ -like MLWF in CaCuO_2 .

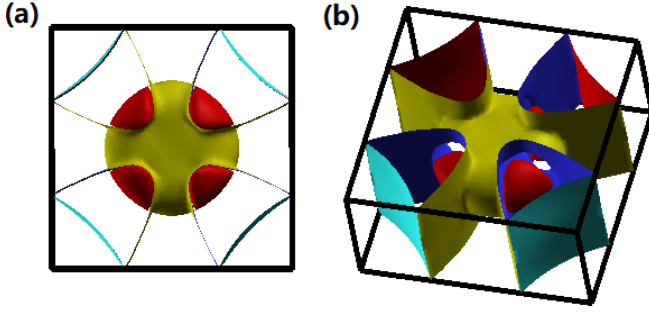


FIG. S5. The Fermi surfaces of BaCuS_2 by Wannier fitting with 4 MLWFs from (a) top view and (b) oblique view.

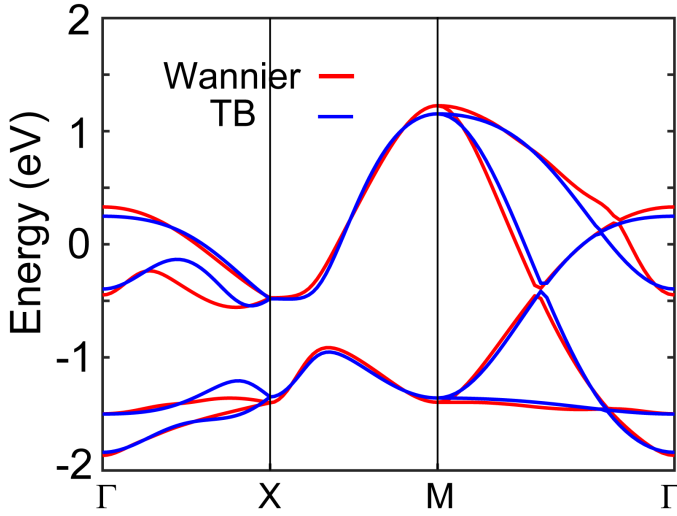


FIG. S6. Comparison of the band structures of BaCuS_2 by Wannierization (red lines) and fitted TB model (blue lines).

TABLE S2. The hopping parameters and on-site energies of in-plane TB model for BaCuS_2 . The energy unit is eV. Here superscript x labels the hopping between two second-nearest-neighbour (SNN) sites along X direction, superscript xx labels the hopping between two forth-nearest-neighbour sites along X direction, superscript xy labels the hopping between two nearest-neighbour (NN) sites along $Y = X$ direction, superscript $xyxy$ labels the hopping between two third-nearest-neighbour (TNN) sites along $Y = X$ direction, superscript xy labels the hopping between two fifth-nearest-neighbour sites along $Y = X/3$ direction; subscript 1-4 represent Cu_A 's $d_{X^2-Y^2}$ orbital, Cu_A 's d_{z^2} orbital, Cu_B 's $d_{X^2-Y^2}$ orbital and Cu_B 's d_{z^2} orbital, respectively.

ε_1	ε_2	t_{11}^x	t_{11}^{xx}	t_{11}^{xyxy}
-0.31	-0.82	-0.28	-0.07	0.15
t_{22}^x	t_{22}^{xx}	t_{22}^{xyxy}	t_{12}^x	t_{12}^{xx}
0.09	0.003	-0.05	-0.08	0.01
t_{13}^{xy}	t_{13}^{xyxy}	t_{24}^{xy}	t_{24}^{xyxy}	t_{14}^{xyxy}
0.25	-0.03	-0.26	0.02	-0.01

Appendix F: U/J parameters calculated by Local screened Coulomb correction (LSCC) approach

The U/J parameters represent the correlation strength in DFT+ U calculations and are often chosen empirically. Here we employ the first-principle LSCC approach[54] to calculate the U/J parameters in layered transition metal compounds CaCuO₂, FeSe, La₃N₃Ni₂B₂, BaNiS₂ and BaCuS₂. In LSCC method, the local Coulomb interactions are calculated by using the Yukawa potential, so the U/J should decrease when the system becomes more metallic. Since the U/J is strongly dependent on the muffin-tin radius R_{MT} , we should only compare the U/J with the same pseudopotential. As shown in TABLE.S3, the U/J is larger when AFM order exists in CaCuO₂/FeSe. The U/J in BaNiS₂ is larger than in La₃N₃Ni₂B₂ because the correlation effect are non-negligible in BaNiS₂[55, 56] and La₃N₃Ni₂B₂ is a typical metal. From this point of view, our results also demonstrate that the correlation in BaCuS₂ is weaker than in cuprate CaCuO₂.

TABLE S3. The U/J parameters and moments calculated by LSCC method.

LSCC	U (eV)	J (eV)	moment (μ_B)
CaCuO ₂ (AFM)	5.78	1.16	0.478
CaCuO ₂ (NM)	5.74	1.16	0
FeSe(CAFM)	4.88	0.91	3.05
FeSe(NM)	4.75	0.89	0
La ₃ N ₃ Ni ₂ B ₂	5.49	0.99	0
BaNiS ₂	5.61	1.01	0
BaCuS ₂	5.7	1.15	0

Appendix G: method of RPA calculation

In this section, we explain the formalism of the multiorbital RPA approach[36, 37, 39, 57, 58], adopted in the main text. The multi-orbital susceptibility is defined as,

$$\chi_{l_1 l_2 l_3 l_4}(\mathbf{q}, \tau) = \frac{1}{N} \sum_{\mathbf{k} \mathbf{k}'} \langle T_\tau c_{l_3 \sigma}^\dagger(\mathbf{k} + \mathbf{q}, \tau) c_{l_4 \sigma}(\mathbf{k}, \tau) c_{l_2 \sigma'}^\dagger(\mathbf{k}' - \mathbf{q}, 0) c_{l_1 \sigma'}(\mathbf{k}', 0) \rangle. \quad (\text{G1})$$

In momentum-frequency space, the multi-orbital bare susceptibility is given by

$$\chi_{l_1 l_2 l_3 l_4}^0(\mathbf{q}, i\omega_n) = -\frac{1}{N} \sum_{\mathbf{k} \mu \nu} a_\mu^{l_4}(\mathbf{k}) a_\mu^{l_2*}(\mathbf{k}) a_\nu^{l_1}(\mathbf{k} + \mathbf{q}) a_\nu^{l_3*}(\mathbf{k} + \mathbf{q}) \frac{n_F(E_\mu(\mathbf{k})) - n_F(E_\nu(\mathbf{k} + \mathbf{q}))}{i\omega_n + E_\mu(\mathbf{k}) - E_\nu(\mathbf{k} + \mathbf{q})}, \quad (\text{G2})$$

where μ and ν are the band indices, n_F is the usual Fermi distribution, l_i ($i = 1, 2, 3, 4$) are the orbital indices, $a_\mu^{l_i}(\mathbf{k})$ is

the l_i orbital component of the eigenvector for band μ resulting from the diagonalization of the tight-binding Hamiltonian H_0 and $E_\mu(\mathbf{k})$ is the corresponding eigenvalue. With interactions, the RPA spin and charge susceptibilities are given by

$$\begin{aligned} \chi_s^{RPA}(\mathbf{q}) &= \chi^0(\mathbf{q})[1 - \bar{U}^s \chi^0(\mathbf{q})]^{-1}, \\ \chi_c^{RPA}(\mathbf{q}) &= \chi^0(\mathbf{q})[1 + \bar{U}^c \chi^0(\mathbf{q})]^{-1}, \end{aligned} \quad (\text{G3})$$

where \bar{U}^s (\bar{U}^c) is the spin (charge) interaction matrix,

$$\bar{U}_{l_1 l_2 l_3 l_4}^s(\mathbf{q}) = \begin{cases} U & l_1 = l_2 = l_3 = l_4, \\ U' & l_1 = l_3 \neq l_2 = l_4, \\ J & l_1 = l_2 \neq l_3 = l_4, \\ J' & l_1 = l_4 \neq l_2 = l_3, \end{cases} \quad (\text{G4})$$

$$\bar{U}_{l_1 l_2 l_3 l_4}^c(\mathbf{q}) = \begin{cases} U & l_1 = l_2 = l_3 = l_4, \\ -U' + 2J & l_1 = l_3 \neq l_2 = l_4, \\ 2U' - J & l_1 = l_2 \neq l_3 = l_4, \\ J' & l_1 = l_4 \neq l_2 = l_3, \end{cases} \quad (\text{G5})$$

In the main text, we plot the largest eigenvalues of the susceptibility matrix $\chi_{l_1 l_1 l_2 l_2}^0(\mathbf{q}, 0)$ and $\chi_{s, l_1 l_1 l_2 l_2}^{RPA}(\mathbf{q}, 0)$. Within RPA approximation, the effective Cooper scattering interaction on Fermi surfaces is,

$$\begin{aligned} \Gamma_{ij}(\mathbf{k}, \mathbf{k}') &= \sum_{l_1 l_2 l_3 l_4} a_{v_i}^{l_2, *}(\mathbf{k}) a_{v_i}^{l_3, *}(-\mathbf{k}) \\ &Re \left[\Gamma_{l_1 l_2 l_3 l_4}(\mathbf{k}, \mathbf{k}', \omega = 0) \right] a_{v_j}^{l_1}(\mathbf{k}') a_{v_j}^{l_4}(-\mathbf{k}'), \end{aligned} \quad (\text{G6})$$

where the momenta \mathbf{k} and \mathbf{k}' is restricted to different FSs with $\mathbf{k} \in C_i$ and $\mathbf{k}' \in C_j$. The orbital vertex function $\Gamma_{l_1 l_2 l_3 l_4}$ in spin singlet channel[59, 60] is

$$\begin{aligned} \Gamma_{l_1 l_2 l_3 l_4}^S(\mathbf{k}, \mathbf{k}', \omega) &= \left[\frac{3}{2} \bar{U}^s \chi_s^{RPA}(\mathbf{k} - \mathbf{k}', \omega) \bar{U}^s + \frac{1}{2} \bar{U}^s \right. \\ &\left. - \frac{1}{2} \bar{U}^c \chi_c^{RPA}(\mathbf{k} - \mathbf{k}', \omega) \bar{U}^c + \frac{1}{2} \bar{U}^c \right]_{l_1 l_2 l_3 l_4}, \end{aligned} \quad (\text{G7})$$

where χ_s^{RPA} and χ_c^{RPA} are the RPA spin and charge susceptibility, respectively. The pairing strength functional for a specific pairing state is given by,

$$\lambda[g(\mathbf{k})] = -\frac{\sum_{ij} \oint_{C_i} \frac{d\mathbf{k}_\parallel}{v_F(\mathbf{k})} \oint_{C_j} \frac{d\mathbf{k}'_\parallel}{v_F(\mathbf{k}')} g(\mathbf{k}) \Gamma_{ij}(\mathbf{k}, \mathbf{k}') g(\mathbf{k}')}{(2\pi)^2 \sum_i \oint_{C_i} \frac{d\mathbf{k}_\parallel}{v_F(\mathbf{k})} [g(\mathbf{k})]^2}, \quad (\text{G8})$$

where $v_F(\mathbf{k}) = |\nabla_{\mathbf{k}} E_i(\mathbf{k})|$ is the Fermi velocity on a given Fermi surface sheet C_i . The pairing vertex function in spin singlet and triplet channels are symmetric and antisymmetric parts of the interaction, that is, $\Gamma_{ij}^{S/T}(\mathbf{k}, \mathbf{k}') = \frac{1}{2} [\Gamma_{ij}(\mathbf{k}, \mathbf{k}') \pm \Gamma_{ij}(\mathbf{k}, -\mathbf{k}')]$.